Ab Initio Molecular Orbital Study of Reactivity of Active Alkyl Groups. III. Nitrosation of Acyclic Carbonyl Compound with Methyl Nitrite *via* Na^+ Chelated Transition State

Tokihiro NIIYA, Hirohito IKEDA, Miho YUKAWA, and Yoshinobu GOTO*

Faculty of Pharmaceutical Sciences, Fukuoka University, Nanakuma, Jonan-ku, Fukuoka 814–80, Japan.
Received January 16, 1997; accepted June 23, 1997

The mechanism of the nitrosation of sodium enolate of acetone $[CH_3COCH_2]^-Na^+$ (1) with methyl nitrite CH_3ONO (2) to give 1-hydroxy-imino-2-oxo-propane $CH_3COCH=NOH$ (3) was studied by the *ab initio* molecular orbital (MO) method. The complex $[CH_3COCH_2NO(OCH_3)]^-Na^+$ (C-II) was first formed from the adduct (C-I) of 1 and 2 through the pericyclic transition state (TS1). Finally, *Z*-hydroxyimino compound (3*Z*) was obtained through demethoxylation of 2 moiety and abstraction of an active hydrogen atom in C-II with a base. In the final formation of 3*Z*, two leaving groups, the methoxy group and the active hydrogen atom in C-II, should be situated in positions with respect to each other which permit their elimination, *i.e.*, they are antiperiplanar to one another. It has become apparent that 3*Z* tends to be formed predominantly when a countercation of a base coordinates to the oxygen atom of the enolate of acetone.

Key words *ab initio* MO method; reaction mechanism; active alkyl group; nitrosation; pericyclic transition state; antiperiplanar transition state

Electrophilic displacement reaction of active alkyl compounds ($RCOCH_3$) with electrophilic reagents (E^+) using base catalysts (B^-M^+) is one of the most important, synthetically useful and fundamental organic reactions. The progress of this reaction is generally shown by Eqs. 1 and 2.

$$RCOCH_3 + B^-M^+ \rightarrow [RCOCH_2]^-M^+ + BH \quad (1)$$

$$[RCOCH_2]^-M^+ + E^+ \rightarrow RCOCH_2E + M^+ \quad (2)$$

The rate-determining step of the reaction is influenced by the nature of E^+. For example, in the case of the halogenation or the deuterium exchange reactions, the rate-determining step is Eq. 1, while in that of the nitrosation or the aldol condensation[1] it is Eq. 2. The rate-determining step of nitrosation of $RCOCH_3$ with R′ONO carried out using a base catalyst to give *E*- and *Z*-oxime (Fig. 1) is generally expressed by Eq. 3.

$$[RCOCH_2]^-M^+ + R'ONO \rightarrow RCOCH=NOH + R'OM \quad (3)$$

It is well known that the aldol condensations in an aprotic solvent are highly stereoselective, while the reactions in a protic solvent result in a lowering of the stereoselectivity. To illustrate these results the metal-chelated pericyclic and the open-chain without metal transition states have been proposed, and the stereoselective aldol condensations are successfully explained in terms of the mechanisms *via* the chair-like pericyclic transition states.[2] A pericyclic transition state is believed to exist in an aprotic solvent in preference to an open-chain one, and in a protic solvent that the reverse is true. In addition to these behaviors it is assumed that the effect of the solvation on the transition state in an aprotic solvent is smaller than that in a protic one. In the nitrosation of isovalerophenone $PhCOCH_2CH(CH_3)_2$ (**4**) under protic conditions, *i.e.*, EtONa in EtOH, the yield of *E*-2-hydroxyimino-1-phenyl-3-methyl-1-oxo-butane (**5**) was 2.3 times that of *Z*-oxime (**6**). On the contrary, under aprotic conditions, *i.e.*, lithium diisopropylamide (LDA) in tetrahydrofuran (THF), the ratio of the yield of **5** over that of **6** is 3/4.[3] In the present study, the mechanism of the nitrosation of acetone with methyl nitrite (**2**) in the presence of the base (CH_3O^-) shown in Eq. 4, as a model reaction, was investigated by *ab initio* MO method using Hartree–Fock approximation with 6-31G basis set (HF/6-31G), to determine whether the structure of the desired oxime is the *E*- or *Z*-form, when Na^+ coordinates to the oxygen atom of the enolate of acetone. *Z*-1-Hydroxy-imino-2-oxo-propane (3*Z*) was predominantly obtained when the reaction proceeds *via* the chair-like, Na^+ chelated pericyclic transition state.

$$[CH_3COCH_2]^-Na^+ + CH_3ONO \xrightarrow{CH_3O^-} CH_3COCH=NOH + CH_3ONa \quad (4)$$

Experimental

Computational Procedure The molecular orbital calculations were carried out with the Gaussian 92 program.[4] The optimized geometries in the transition states (TS) were determined with HF/6-31G by the energy gradient method, followed by intrinsic reaction coordinate (IRC) calculations. For energy comparisons of the complexes, single-point calculations were performed on the optimized geometries using a 6-31+G basis set.[5] The electron correlation energy was corrected by the third-order Moeller-Plesset (MP3) perturbation method. The calculation procedure described above is designated MP3/6-31+G//HF/6-31G. In the elimination process, a model in which the oxygen atom of a base CH_3O^- approached the hydrogen atom $H^{1\,(or\,2)}$ along the axis of the $C\text{–}H^{1\,(or\,2)}$ bond was employed.[6] In the determination of the final complex, the calculation from TS using the IRC method was further followed by the geometry optimization under conditions in which the angle $\angle C^1C^2H^{1\,(or\,2)}$ and the dihedral angle $\angle O^1C^1C^2H^{1\,(or\,2)}$ in path H^1 and H^2 were fixed at 90° in the same way as reported previously,[6] respectively (see Table 4).

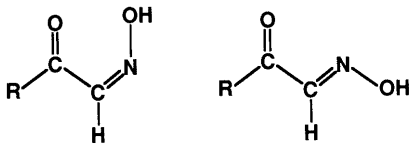

Z-oxime *E*-oxime

Fig. 1

* To whom correspondence should be addressed.

Results and Discussion

In the deprotonation of ethyl methyl ketone (EMK), a proton of the methyl group reacts more easily with alkoxide anion than that of methylene of the ethyl group of EMK.[6] The nitrosation reaction of EMK with R'ONO in the presence of a base, however, results in the formation of 2-hydroxyimino-3-oxo-butane (**7**) exclusively.[7] This result indicates that the rate-determining step in the nitrosation is the C–N bond formation process, and that R'ONO reacted with a thermodynamically stable enolate $[CH_3COCHCH_3]^-Na^+$ produced by abstraction of an active hydrogen atom on the carbon adjacent to the carbonyl group to give **7**.

The present report describes the study of the mechanism of nitrosation of **1** with **2** to give **3** by the method of MO calculation using the HF/6-31G. The MO calculation for the formation of **3** was carried out stepwise as follows: Eq. 4 was divided into two steps, and the MO calculation for the first step (C–N bond formation) expressed by Eq. 5 was performed, followed by that for the second step (elimination) expressed by Eq. 6. In the former step, the complex (C-I) of **1** with **2** is formed, and then *via* the TS (TS1) the complex (C-II) is obtained. In the latter one, CH_3O^- approaches the hydrogen atom of C-II to form the complex (C-III), and through the TS (TS2) the final complex (C-IV) is produced.

C–N Bond Formation of the Enolate of Acetone with Methyl Nitrite The following reaction model of the C–N bond formation step in the nitrosation was adopted: the geometrical orientation of methyl nitrite[8,9] with respect to the carbanion of acetone is believed to be as shown in Fig. 2.

The interrupted arrow in the figure denotes the direction of methyl nitrite molecule to the active center carbon having the largest charge density in HOMO of **1**. As shown, **2** approached **1** along the axis between the nitrogen atom of **2** and the carbon atom (C^2) of **1** by rotating **2** around the axis C^2–N. The energy calculation of the reaction through path A (Fig. 3) was performed using the orientation of **2** shown in Fig. 2a, whereas calculation of reaction path B (Fig. 3) was carried out with the orientation of **2** shown in Fig. 2b. The optimized conformations of TS1 were first determined, and those of C-I and C-II were next obtained from the TS1 using the IRC method. Although TS1 which has a coordinate bond between Na^+ ion and O^3 atom would be predictable from the coordination complex C-I, the complex finally settled down at the transition state, in which Na^+ ion coordinates not to O^3 but to O^2 atom. The calculated energies ($E_{C\text{-}I}$, E_{TS1}, $E_{C\text{-}II}$) and the optimized geometries of complexes in the C–N bond formation are presented in Table 1 and 2, respectively.

The energy difference between TS1-A (or TS1-B) and C-I calculated at the MP3/6-31+G//HF/6-31G level is

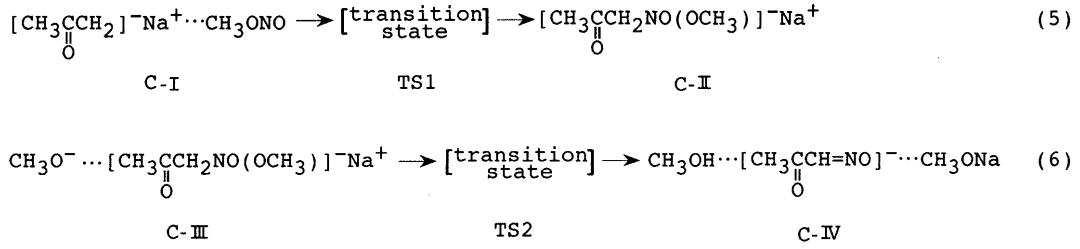

Chart 1

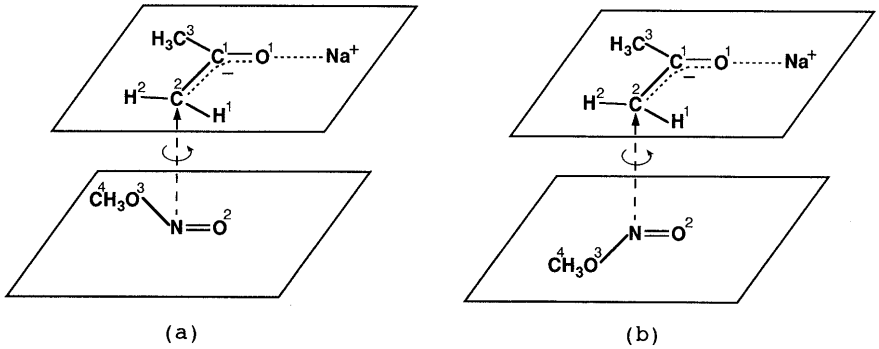

Fig. 2. Orientation of Methyl Nitrite towards Sodium Enolate of Acetone for Energy Calculation of C–N Bond Formation

Table 1. Calculated Energies of Complexes in Path A and B (a.u.)

Method	$E_{C\text{-}I}$	Path A		Path B	
		$E_{TS1\text{-}A}$	$E_{C\text{-}II\text{-}A}$	$E_{TS1\text{-}B}$	$E_{C\text{-}II\text{-}B}$
HF/6-31G	−596.69506	−596.68522	−596.74147	−596.68204	−596.72843
HF/6-31+G//HF/6-31G	−596.73143	−596.70201	−596.75764	−596.69870	−596.74733
MP3/6-31+G//HF/6-31G	−597.56941	−597.56077	−597.63294	−597.56028	−597.62432

Table 2. Optimized Geometries of Complexes in Path A and B

Geometric parameter	C-I	Path A		Path B	
		TS1-A	C-II-A	TS1-B	C-II-B
Bond length (Å)					
$r(C^1–O^1)$	1.328	1.279	1.227	1.275	1.233
$r(C^1–C^2)$	1.343	1.394	1.513	1.398	1.509
$r(C^2–H^1)$	1.075	1.072	1.082	1.073	1.084
$r(C^2–H^2)$	1.073	1.073	1.085	1.072	1.078
$r(C^1–C^3)$	1.511	1.505	1.504	1.506	1.495
$r(C^3–H^3)$	1.086	1.086	1.083	1.084	1.079
$r(C^3–H^4)$	1.082	1.081	1.086	1.085	1.084
$r(C^3–H^5)$	1.086	1.082	1.079	1.080	1.085
$r(C^2–N)$	6.056	2.136	1.454	2.126	1.469
$r(N–O^2)$	1.178	1.243	1.407	1.248	1.397
$r(N–O^3)$	1.370	1.413	1.499	1.415	1.448
$r(O^3–C^4)$	1.471	1.433	1.428	1.433	1.425
$r(C^4–H^6)$	1.077	1.080	1.081	1.079	1.083
$r(C^4–H^7)$	1.076	1.079	1.081	1.080	1.078
$r(C^4–H^8)$	1.077	1.077	1.081	1.077	1.080
$r(O^1–Na)$	1.987	2.093	2.145	2.107	2.239
Bond angle (°)					
$\angle O^1C^1C^2$	124.5	122.4	124.7	122.1	121.1
$\angle C^1C^2H^1$	120.9	118.7	108.0	117.7	110.8
$\angle C^1C^2H^2$	121.8	119.9	107.5	119.1	110.7
$\angle O^1C^1C^3$	114.4	116.8	119.8	117.1	120.8
$\angle C^1C^3H^3$	109.7	108.8	111.7	109.3	110.7
$\angle C^1C^3H^4$	112.7	112.7	109.0	109.2	109.0
$\angle C^1C^3H^5$	109.6	109.4	110.1	112.6	110.3
Bond angle (°)					
$\angle C^1C^2N$	66.8	100.0	118.9	100.1	107.2
$\angle C^2NO^2$	119.6	106.3	110.3	107.4	109.0
$\angle C^2NO^3$	13.1	104.5	105.0	96.9	101.7
$\angle NO^3C^4$	115.7	112.3	109.7	112.6	110.4
$\angle O^3C^4H^6$	108.7	110.3	110.2	110.6	110.4
$\angle O^3C^4H^7$	103.5	110.5	110.4	110.3	110.1
$\angle O^3C^4H^8$	108.7	105.5	107.0	105.6	106.0
$\angle C^1O^1Na$	173.9	126.6	94.0	123.3	116.7
Dihedral angle (°)					
$\angle O^1C^1C^2H^1$	−2.5	−20.3	−133.2	−20.7	−37.0
$\angle O^1C^1C^2H^2$	179.5	−172.9	111.1	−171.2	−159.2
$\angle C^2O^1C^1C^3$	179.3	172.8	180.0	173.8	177.6
$\angle O^1C^1C^3H^3$	−57.8	−70.0	−139.0	56.4	−2.1
$\angle O^1C^1C^3H^4$	−179.3	169.4	102.3	−60.8	−123.2
$\angle O^1C^1C^3H^5$	59.5	47.6	−16.8	178.1	119.3
$\angle O^1C^1C^2N$	22.1	73.7	−13.2	78.2	82.8
$\angle C^1C^2NO^2$	−49.5	−58.5	−51.9	−45.4	−75.9
$\angle C^1C^2NO^3$	3.0	55.9	64.0	−156.8	170.0
$\angle O^2NO^3C^4$	180.0	−167.6	−115.9	167.5	72.6
$\angle NO^3C^4H^6$	−59.7	47.6	56.7	80.9	61.3
$\angle NO^3C^4H^7$	−179.0	−74.2	−64.0	−41.0	−60.1
$\angle NO^3C^4H^8$	61.7	−166.7	176.7	−160.1	−179.5
$\angle C^2C^1O^1Na$	45.5	−51.8	90.4	−51.9	−37.5

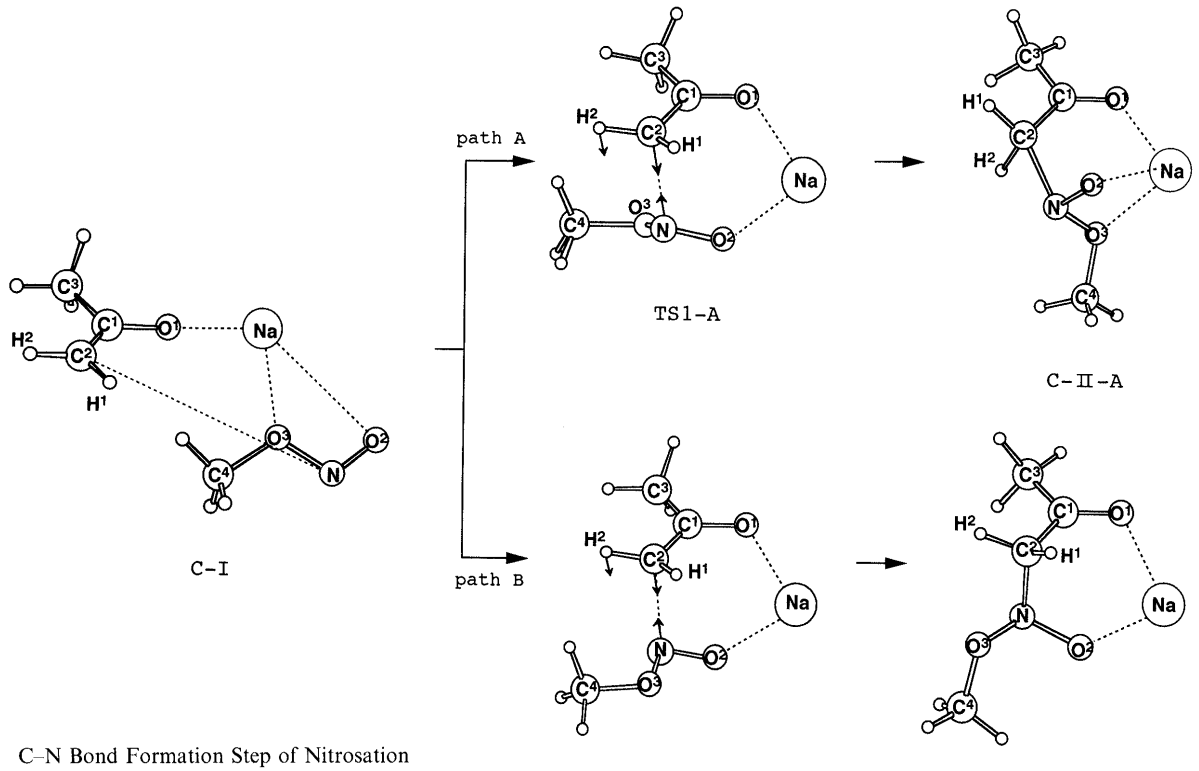

Fig. 3. C–N Bond Formation Step of Nitrosation

Imaginary frequency modes are shown with bold arrows in the structures of the transition states.

Table 3. Calculated Energies of Complexes in Path H^1 and H^2 (a.u.)

Method	Path H^1			Path H^2		
	$E_{C\text{-III-}H^1}$	$E_{TS2\text{-}H^1}$	$E_{C\text{-IV-}H^1}$	$E_{C\text{-III-}H^2}$	$E_{TS2\text{-}H^2}$	$E_{C\text{-IV-}H^2}$
HF/6-31G	−711.10676	−711.10628	−711.22984	−711.12104	−711.11356	−711.14779
HF/6-31+G//HF/6-31G	−711.13983	−711.13840	−711.26278	−711.15296	−711.14309	−711.17856
MP3/6-31+G//HF/6-31G	−712.26130	−712.26237	−712.32230	−712.27305	−712.26781	−712.30076

Table 4. Optimized Geometries of Complexes in Path H^1 and H^2

Geometric parameter	Path H^1			Path H^2		
	C-III-H^1	TS2-H^1	C-IV-H^1	C-III-H^2	TS2-H^2	C-IV-H^2
Bond length (Å)						
r(C^1–O^1)	1.240	1.239	1.247	1.238	1.254	1.312
r(C^1–C^2)	1.499	1.493	1.431	1.501	1.449	1.360
r(C^2–H^1)	1.134	1.153	2.459	1.084	1.085	1.073
r(C^2–H^2)	1.086	1.085	1.070	1.111	1.328	2.426
r(C^1–C^3)	1.504	1.506	1.513	1.506	1.513	1.517
r(C^3—H^3)	1.087	1.086	1.081	1.085	1.082	1.083
r(C^3–H^4)	1.087	1.086	1.086	1.085	1.086	1.086
r(C^3–H^5)	1.081	1.081	1.081	1.081	1.081	1.086
r(C^2–N)	1.455	1.454	1.325	1.458	1.461	1.439
r(N–O^2)	1.384	1.336	1.275	1.412	1.416	1.413
r(N–O^3)	1.595	1.738	5.228	1.509	1.521	1.564
r(O^3–C^4)	1.416	1.407	1.378	1.435	1.424	1.417
r(C^4–H^6)	1.084	1.088	1.103	1.083	1.083	1.084
r(C^4–H^7)	1.084	1.088	1.103	1.083	1.083	1.084
r(C^4–H^8)	1.084	1.088	1.103	1.083	1.083	1.084
r(O^2–Na)	2.128	2.148	2.245	2.127	2.135	2.143
r($H^{1(2)}$–O^4)	1.676	1.606	0.953	1.787	1.293	0.959
r(O^4–C^5)	1.390	1.391	1.433	1.387	1.399	1.424
r(C^5–H^9)	1.104	1.103	1.081	1.106	1.097	1.082
r(C^5–H^{10})	1.104	1.103	1.081	1.106	1.097	1.082
r(C^5–H^{11})	1.104	1.103	1.081	1.106	1.097	1.082
Bond angle (°)						
∠$O^1C^1C^2$	127.3	127.5	125.9	127.4	127.7	128.1
∠$C^1C^2H^1$	103.1	103.5	90.0	108.2	109.5	119.3
∠$C^1C^2H^2$	107.1	107.6	118.0	102.5	103.9	90.0
∠$O^1C^1C^3$	119.9	119.7	117.5	119.6	117.5	114.2
∠$C^1C^3H^3$	109.8	109.9	112.6	108.5	110.3	113.3
∠$C^1C^3H^4$	108.3	108.3	109.1	109.8	109.3	108.6
∠$C^1C^3H^5$	110.4	110.3	109.2	110.4	109.8	109.6
∠C^1C^2N	120.5	120.8	127.9	120.2	121.5	128.9
∠C^2NO^2	113.7	114.1	121.2	112.0	112.9	116.3
∠C^2NO^3	103.0	100.3	100.9	104.6	106.1	106.0
∠NO^3C^4	107.9	107.4	167.2	110.3	110.6	107.4
∠$O^3C^4H^6$	110.0	110.8	113.6	108.7	109.0	109.6
∠$O^3C^4H^7$	110.0	110.8	113.6	108.7	109.0	109.6
∠$O^3C^4H^8$	110.0	110.8	113.6	108.7	109.0	109.6
∠NO^2Na	93.4	94.3	136.7	91.5	90.1	89.0
∠$C^1C^2O^4$	103.1	103.5	90.0	102.5	103.9	90.0
∠$C^2O^4C^5$	116.1	116.7	110.9	117.6	115.2	110.9
∠$O^4C^5H^9$	113.6	113.5	109.9	113.9	112.6	110.1
∠$O^4C^5H^{10}$	113.6	113.5	109.9	113.9	112.6	110.1
∠$O^4C^5H^{11}$	113.6	113.5	109.9	113.9	112.6	110.1
Dihedral angle (°)						
∠$O^1C^1C^2H^1$	−138.3	−134.1	−90.0	−121.8	−141.4	−180.4
∠$O^1C^1C^2H^2$	112.0	116.1	175.3	125.1	111.7	90.0
∠$C^2O^1C^1C^3$	180.0	180.0	180.0	180.0	180.0	180.0
∠$O^1C^1C^3H^3$	−113.0	−113.4	−157.2	−127.6	−135.2	−178.8
∠$O^1C^1C^3H^4$	130.5	129.6	82.7	114.8	105.6	60.0
∠$O^1C^1C^3H^5$	7.5	7.1	−34.9	−5.8	−13.9	−56.8
∠$O^1C^1C^2N$	−11.3	−7.7	−2.9	0.4	−15.4	−6.0
∠$C^1C^2NO^2$	−51.9	−48.5	−2.2	−55.1	−49.6	−53.2
∠$C^1C^2NO^3$	65.1	63.5	−1.2	59.8	65.2	61.9
∠$C^2NO^3C^4$	−116.5	−127.0	9.3	−149.3	−143.6	−92.8
∠$NO^3C^4H^6$	56.0	54.8	36.4	57.8	53.3	53.5
∠$NO^3C^4H^7$	−63.5	−64.9	−83.5	−62.7	−67.2	−66.4
∠$NO^3C^4H^8$	176.7	175.4	156.5	177.2	172.8	173.9
∠C^2NO^2Na	84.2	83.9	5.3	87.3	84.5	74.7
∠$O^1C^1C^2O^4$	−138.3	−134.1	−90.0	125.1	111.7	90.0
∠$C^1C^2O^4C^5$	93.0	88.1	85.2	134.8	136.2	−52.2
∠$H^{1(2)}O^4C^5H^9$	−4.9	−3.8	53.7	−3.1	−6.6	−70.7
∠$H^{1(2)}O^4C^5H^{10}$	115.1	116.1	173.8	116.9	113.3	49.0
∠$H^{1(2)}O^4C^5H^{11}$	−125.3	−124.2	−66.4	−123.1	−126.6	169.0

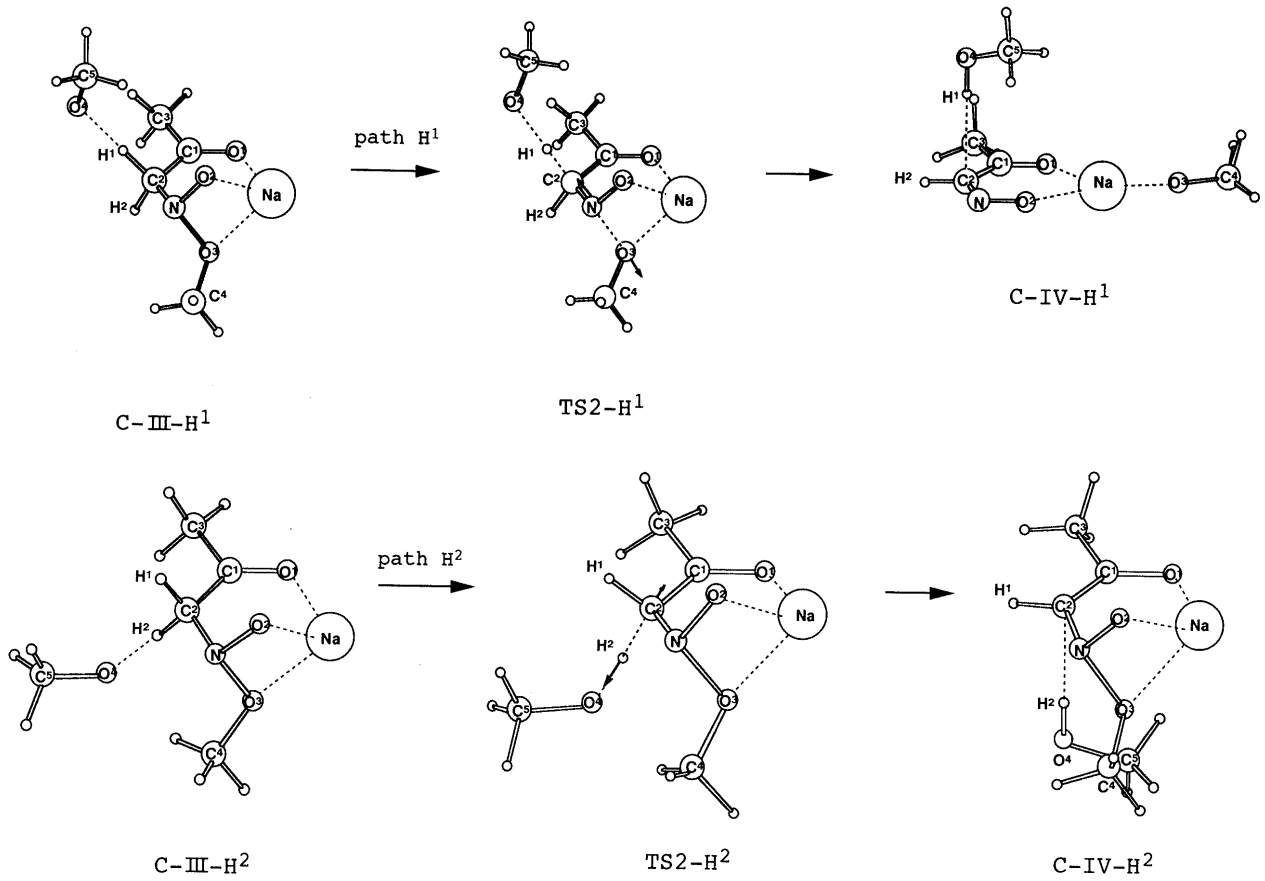

Fig. 4. Elimination Step of Nitrosation

Imaginary frequency modes are shown with bold arrows in the structures of the transition states.

0.0086 (or 0.091) a.u. (5.4 (or 5.7) kcal mol^{-1}) as shown in Table 1.

The C–N bond formation *via* path A and B is shown in Fig. 3. In both paths, a 6-membered ring is formed in the TS1, which includes Na^+ ion. This TS is similar to that in the aldol-condensation reaction proposed by Zimmerman and Traxler.[2a] In the process from C-I to C-II, the structure of **1** changes from the enol- to the keto-form (Table 2).

The structure of C-II-A is more energetically stable than that of C-II-B. Consequently, the reaction path from C-II-A to the desired oxime was investigated further.

Elimination of Proton and Methoxide in C-II-A with a Base Another base CH_3O^- also approaches C-II-A, followed by the formation of C-III. The following elimination model in the formation of the oxime was adopted: the oxygen atom of CH_3O^- approaches the hydrogen atom $H^{1\,(or\,2)}$ along the axis between the oxygen atom of CH_3O^- and the hydrogen atom of the C^2–$H^{1\,(or\,2)}$ bond, *i.e.*, path H^1 and H^2 (Fig. 4). The optimized conformations of the TS2 were first determined, and then those of C-III and C-IV were obtained from the TS2 using IRC method. The calculated energies ($E_{C\text{-III}}$, E_{TS2}, $E_{C\text{-IV}}$) of C-III, TS2 and C-IV, and their optimized geometries are shown in Tables 3 and 4, respectively. The elimination process *via* path H^1 and H^2 is shown in Fig. 4.

It is well known that E2 reactions occur readily from an anti-periplanar geometry, meaning that the leaving groups lie in the same plane,[10] and now in the present study two leaving groups, H^1 and CH_3O^3, which are periplanar, depart easily from opposite sides of the complexes, C-III-H^1 and TS2-H^1. As shown in Table 4, both the C^2–H^1 and N–O^3 bond lengths in C-III-H^1 are longer than those in C-II-A, and these lengths became even longer with the approach of CH_3O^- close to H^1. Further, C-III-H^1 changed into C-IV-H^1 *via* TS2-H^1, and it can be seen in Fig. 4 that in C-IV-H^1 the desired *Z*-form of the hydroxyimino compound (*Z*-oxime) is already formed.

Table 5. Relative Energies of Complexes in Path A, B, H^1 and H^2 on the Basis of Calculated Energy of C-I (kcal mol^{-1})

	TS1	C-II		C-III	TS2	C-IV
Path A	5.4	−39.9	Path H^1	−55.2	−55.9	−93.5
			Path H^2	−62.6	−59.3	−79.9
Path B	5.7	−34.5				

The two leaving groups, H^2 and CH_3O^3 in C-III-H^2 and TS2-H^2, are not antiperiplanar but gauche as shown in the figure, and in spite of lengthening of the C^2–H^2 bond with the approach of CH_3O^-, the N–O^3 bond does not become longer in either TS2-H^2 or C-IV-H^2, *i.e.*, the desired *Z*-oxime cannot be formed, when CH_3O^- approaches H^2 in C-II-A (*cf.* Table 4).

Each relative energy of the complexes in path A, B, H^1 and H^2 calculated on the basis of the energy of C-I is shown in Table 5. The reaction profiles for the C–N bond formation and the elimination of proton and methoxide in the nitrosation of **1** with **2** are depicted in Fig. 5 using the energy values in Table 5. The reaction profiles in this figure show that the nitrosation proceeds readily from C-I

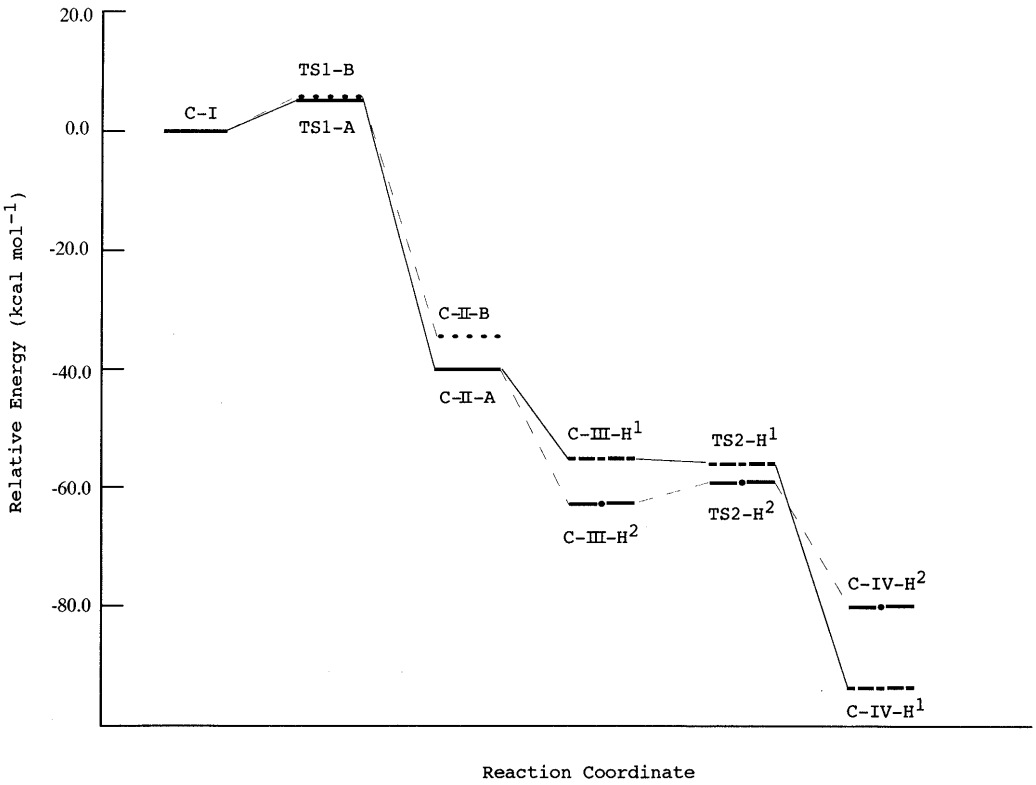

Fig. 5. Reaction Profiles for the C–N Bond Formation and the Elimination of Proton and Methoxide in the Nitrosation of Sodium Enolate of Acetone with Methyl Nitrite

The calculations of all energies were carried out using MP3/6-31+G//HF/6-31G. Path A, ——; path B, ------; path H^1, — — —; path H^2, —·—.

via the reaction path as depicted by a solid line to the last complex C-IV-H^1, *i.e.* *Z*-oxime.

It is concluded that the *Z*-oxime is obtained when the nitrosation proceeds *via* the chair-like, Na^+ chelated pericyclic transition state. Actually, in the case of the nitrosation of simple carbonyl compounds, such as acetone, EMK, *etc.*, only the *E*-form of hydroxyimino compound (*E*-oxime) is obtained exclusively. *Z*-Oxime would readily change into *E*-oxime, even if the former were formed in the course of the nitrosation process. In the case of the treatment of carbonyl compounds having a bulky alkyl group with R′ONO, however, both *E*- and *Z*-oxime are obtained simultaneously, and the ratio of *E*- and *Z*-oxime is variable depending on the kinds of catalysts and solvents as described above.[3)]

A chair-like, Na^+ chelated pericyclic transition state tends to be formed in the course of the nitrosation process under aprotic conditions. Recently, preliminary MO investigations revealed that the *E*-oxime is readily formed when the nitrosation proceeds without Na^+-coordination. Details on this will be reported in the near future.

Acknowledgements Thanks are due to the Computational Center of Fukuoka University for use of the FACOM M780/10S and NEC SX3/11R computers, and to the Computer Center of the Institute for Molecular Science, Okazaki National Research Institutes for use of the HITAC S810/10, and NEC HSP computers.

References and Notes

1) House H. O., "Modern Synthetic Reactions," 2nd ed., Benjamin W. A., Menlo Park, Calif., 1972, pp. 629—682.
2) *a*) Zimmerman H. E., Traxler M. D., *J. Am. Chem. Soc.*, **79**, 1920—1923 (1957); *b*) Dubois J. E., Fort J. F., *Tetrahedron*, **28**, 1653—1663 (1972); *c*) Dubois J. E., Fellman P., *Tetrahedron Lett.*, **1975**, 1225—1228; *d*) Heathcock C. H., "Asymmetric Synthesis," Vol 3, ed. by Morrison J. D., Academic Press Inc., Orlando, 1984, pp. 111—212; *e*) Heathcock C. H., Buse C. T., Kleschick W. A., Pirrung M. C., Sohn J. E., Lampe J., *J. Org. Chem.*, **45**, 1066—1081 (1980); *f*) Evans D. A., Nelson J. V., Vogel E., Taber T. R., *J. Am. Chem. Soc.*, **103**, 3099—3111 (1981); *g*) Li Yi, Paddon-Row M. N., Houk K. N., *J. Org. Chem.*, **55**, 481—493 (1990); *h*) Gennari C., Vieth S., Comotti A., Vulpetti A., Goodman J. M., Paterson I., *Tetrahedron*, **48**, 4439—4458 (1992); *i*) Vulpetti A., Bernardi A., Gennari C., Goodman J. M., Paterson I., *ibid.*, **49**, 685—696 (1993).
3) Formation of *E*- (**5**) and *Z*-2-hydroxyimino-1-phenyl-3-methyl-1-oxo-butane (**6**). Protic conditions: isovalerophenone (**4**) (0.02 mol), *tert*-butyl nitrite (0.03 mol), NaOEt (0.08 mol) in EtOH (40 ml). Reaction temperature 0 °C. Yield: **5** (14%), **6** (6%). Aprotic conditions: **4** (0.02 mol), *tert*-butyl nitrite (0.03 mol), LDA (0.022 mol) in THF (40 ml). Reaction temperature 0 °C. Yield: **5** (3%), **6** (4%). All product yields were determined by HPLC.
4) Frisch M. J., Trucks G. W., Head-Gordon M., Gill P. M. W., Wong M. W., Foresman J. B., Johnson B. G., Schlegel H. B., Robb M. A., Replogle E. S., Gomperts R., Andres J. L., Raghavachari K., Binkley J. S., Gonzalez C., Martin R. L., Fox D. J., Defrees D. J., Baker J., Stewart J. J. P., Pople J. A., *Gaussian 92*, Revision A; Gaussian, Inc., Pittsburgh, PA, 1992.
5) Radom L., "Applications of Electronic Structure Theory," ed. by Schaefer H. F., III., Plenum Press, New York, 1977, 333—356.
6) Niiya T., Yukawa M., Morishita H., Ikeda H., Goto Y., *Chem. Pharm. Bull.*, **39**, 2475—2482 (1991).
7) *a*) Semon W. L., Damerell V. R., "Org. Syntheses," Coll. Vol. II, ed. by Blatt A. H., John Wiley & Sons, Inc., New York, 1943, pp. 204—208; *b*) Bartnik R., Orlowska B., *Polish J. Chem.*, **62**, 151–157 (1988).
8) For the MO calculation the *trans*-form of methyl nitrite was adopted, because *tert*-butyl nitrite (*trans*-form) is always used in our experiments, although the *cis*-form of methyl nitrite is slightly more stable than the *trans*-form.[9)]
9) Pawar D., Mark H. L., Hosseini H., Harris Y., Noe E. A., *J. Phys. Chem.*, **97**, 7480—7483 (1993).
10) Gronert S., *J. Am. Chem. Soc.*, **114**, 2346—2354 (1992).